Trajectory Generation for Noise-Constrained Autonomous Flight Operations

Kasey A. Ackerman* and Irene M. Gregory†
NASA Langley Research Center, Hampton, VA, 23681

One of the major factors in acceptance of aircraft operating in urban areas is noise. In this work, we build on a framework for trajectory generation in order to account for limits on acoustic metrics at one or more observer locations. The spatial trajectories are generated using Bézier polynomials and satisfy dynamic, acoustic, and mission constraints. The trajectories also guarantee spatial or temporal separation between vehicles for multi-vehicle operations. A simulation example is provided that demonstrates the reduction in noise levels at a set of measurement locations.

I. Nomenclature

$\boldsymbol{x}$	=	Position in $\mathbb{R}^3$
V	=	Vehicle speed
a_t	=	Total acceleration
a_p	=	Tangential acceleration
m	=	Vehicle mass
t	=	Time
$\hat{t}$	=	Normalized time
γ	=	Flight path angle
χ	=	Ground track
T	=	Net thrust of vehicle propellers
D	=	Aerodynamic drag force
σ	=	Parametric speed
ζ	=	Path parameter
θ	=	Timing law
K_T	=	Thrust coefficient
K_D	=	Drag coefficient
d_p	=	Propeller diameter
ω_p	=	Propeller angular speed
N_p	=	Number of propellers
ω_p	=	Rotor angular rotation rate
c	=	Speed of sound
r	=	Distance between acoustic source and observer
M_t	=	Rotor tip Mach number
$OASPL$	=	Overall Sound Pressure Level
$\mathcal{A}$	=	Acoustic observer location
$\beta_{\mathcal{A}}$	=	Equivalent acoustic metric
b_n^k	=	k-th Bernstein basis function for a polynomial of degree n

II. Introduction

One of the major barriers to public acceptance facing Urban Air Mobility (UAM) and the widespread use of UAM-class vehicles in urban areas is noise management [1]. A variety of approaches to noise mitigation for propeller/rotor driven UAM-class vehicles have been increasingly explored in recent years, including configuration

*Pathways Intern, Dynamic Systems and Control Branch, AIAA Student Member.
†Senior Technologist for Advanced Control Theory and Application, Dynamic Systems and Control Branch, AIAA Associate Fellow.

design [2], trajectory design [3, 4], and directivity control through propeller phase synchronization [5]. Application of hierarchical control to noise mitigation is an attractive option that can be applied to existing vehicles with no modifications to the configuration. The first layer of hierarchical control is to design the vehicle's spatial trajectory to reduce the noise signature at sensitive areas. In practice, such a trajectory design should guarantee separation from any other air traffic while accounting for the airspace, the dynamic limitations of the vehicle, and other relevant restrictions. The second layer involves directivity through rotor phase synchronization. Initial closed loop control work in this area is presented in Ref. [6]. It is anticipated that integrated dynamic trajectory and directivity control in a hierarchical control architecture will provide a flexible tool for noise management of UAM-class vehicles in urban environment.

In this work the authors formulate an acoustic metric and a constraint function that are then used in a multi-vehicle trajectory generation framework [7, 8]. In this framework, trajectories are generated that satisfy constraints on dynamics, mission-specific constraints, and inter-vehicle separation constraints. The vehicle dynamics are differentially flat, allowing the constraint functions to be written in terms of the spatial path and timing law governing the vehicle's progression along the path. The path and constraints are formulated as Bézier curves that provide numerical robustness and efficient algorithms associated with the polynomial Bernstein basis [9]. Additionally, the polynomial representation guarantees the satisfaction of all constraints by avoiding discretization of the trajectory and constraint functions. The acoustic metric and constraint function are formulated in the form of a Bézier curve which allows incorporation of the constraint into the trajectory generation framework. The acoustic metric can also be incorporated into the cost function as a multi-objective optimization problem. This approach is evaluated in a simulation of a UAM-class representative vehicle equipped with multiple propellers in a forward flight configuration [10]. Simulation results demonstrated the acoustic benefits obtained from incorporating the acoustic model in the trajectory generation.

In the remainder of this document, Section III describes the vehicle dynamics along the trajectory and the formulation of the trajectory in terms of Bézier curves. Section IV provides the acoustic model and formulates the acoustic constraint. Simulation examples are shown in Section V, and concluding remarks are made in Section VI.

III. Vehicle Dynamics and Trajectory Definition

A. Vehicle Dynamics

The targeted application for this noise management approach is distributed-propulsion UAM-class vehicles that exhibit complex nonlinear dynamics. However, for the purpose of trajectory generation, it is sufficient to utilize a highly simplified set of dynamics along the desired spatial path and rely on a path-following control law to ensure close tracking of the desired trajectory. The simplified dynamics used for trajectory generation are

$$\dot{\boldsymbol{x}}(t) = V(t) \begin{bmatrix} \cos(\gamma(t))\cos(\chi(t)) \\ \cos(\gamma(t))\sin(\chi(t)) \\ -\sin(\gamma(t)) \end{bmatrix} \tag{1}$$

$$m\dot{V}(t) = T(t) - D(t), \tag{2}$$

where V is the (scalar) speed, the thrust and drag forces act along the velocity vector of the vehicle, and the gravitational force is canceled by lift from the vehicle's aerodynamic surfaces. In effect, this is a simplified fixed-wing aircraft case, where any thrust acting parallel to the lift vector is neglected and only for the component of thrust necessary to overcome aerodynamic drag is accounted for. It is also assumed that the thrust and drag forces can be represented by quadratic polynomials of propeller speed and airspeed, respectively. Specifically,

$$T(t) = K_T\left(V(t)\right)\omega_p^2 \tag{3}$$

$$D(t) = \frac{1}{2}\rho S C_D V(t)^2 = K_D V(t)^2, \tag{4}$$

where ρ is the density of air, S is the wetted area of the vehicle, C_D is the drag coefficient, and $K_T(\cdot)$ is a monotonic polynomial function of the airspeed, V. The wetted area, drag coefficient, and air density are approximated here as constant values.

The vehicle dynamics are subject to a subset of the following constraints:

$$V_{\min} \le V(t) \le V_{\max}, \qquad |a_{\mathrm{t}}(t)| \le a_{\mathrm{t,max}}, \qquad |a_{\mathrm{p}}(t)| \le a_{\mathrm{p,max}}, \tag{5}$$

$$\gamma_{\min} \le \gamma(t) \le \gamma_{\max}, \qquad |\dot{\gamma}(t)| \le \dot{\gamma}_{\max}, \qquad |\dot{\chi}(t)| \le \dot{\chi}_{\max}, \tag{6}$$

$$\omega_{p,\min} \le \omega_p(t) \le \omega_{p,\max}. \tag{7}$$

for all $t \in [0, t_\mathrm{f}]$.

B. Trajectory Definition

We build upon the trajectory generation framework in [7, 9], and define the desired spatial path, $\boldsymbol{x}_d : [0,1] \to \mathbb{R}^3$, as a Pythagorean-hodograph (PH) Bézier curve*,

$$\boldsymbol{x}_d(\zeta) = \sum_{k=0}^{5} \bar{\boldsymbol{x}}_{d,k} b_k^5(\zeta), \tag{8}$$

and the timing law, $\theta : [0,1] \to \mathbb{R}$, which determines the temporal component of the trajectory, as a Bézier curve,

$$\theta(\hat{t}) = \frac{\mathrm{d}\zeta(\hat{t})}{\mathrm{d}\hat{t}} = \sum_{k=0}^{w} \bar{\theta}_k b_k^2(\hat{t}), \tag{9}$$

where $\hat{t}$ is the normalized time $\hat{t} = t/t_\mathrm{f}$ and $\zeta(\hat{t}) : [0,1] \to [0,1]$ is a a dimensionless path parameter expressed as a function of the normalized time $\hat{t}$. The timing law is related to the parametric speed of the vehicle by

$$\sigma(\zeta) = \left\| \boldsymbol{x}_d'(\zeta) \right\|. \tag{10}$$

Since x_d is a PH curve, the norm of its parametric derivative satisfies $(x_d')^\mathsf{T} x_d = \sigma^2$ and σ therefore has an analytic polynomial expression. Definitions and select properties of Bézier curves are provided in the appendix. Additional information regarding Bézier curves and their properties may be found in [11]. Defining the desired trajectory in terms of Bézier curves and leveraging the differential flatness of the simplified dynamics to express the constraint functions as rational Bézier curves, it is possible to enforce the dynamic, acoustic, and mission-specific constraints without computing the function values at (a potentially large number of) discrete points along the trajectory. This can be done by using the computationally-friendly algorithms associated with Bézier curves, in particular the distance algorithm from [12] which enables constraint function extrema to be computed to arbitrary precision without discretization.

Following [9], the equivalent set of constraints in Bézier form is:

$$V_{\min} \le V(t) \le V_{\max}, \qquad a_\mathrm{t}^2(t) \le a_{\mathrm{t,max}}^2, \qquad |a_\mathrm{p}(t)| \le a_{\mathrm{p,max}}, \tag{11}$$

$$\sin\gamma_{\min} \le \sin\gamma(t) \le \sin\gamma_{\max}, \qquad \dot{\gamma}^2(t) \le \dot{\gamma}_{\max}^2, \qquad |\dot{\chi}(t)| \le \dot{\chi}_{\max}, \tag{12}$$

$$T_{\min} \le T(t) \le T_{\max}. \tag{13}$$

The constrained variables can be written in terms of the spatial path and timing law as

$$V(\hat{t}) = \frac{1}{t_\mathrm{f}} \sigma(\zeta(\hat{t}))\theta(\hat{t}) = \sum_{k=0}^{14} \bar{V}_k b_k^{14}(\hat{t}) \tag{14}$$

$$a_\mathrm{p}(\hat{t}) = \frac{1}{t_\mathrm{f}^2} \left(\sigma'(\zeta(\hat{t}))\theta^2(\hat{t}) + \sigma(\zeta(\hat{t}))\theta'(\hat{t}) \right) = \sum_{k=0}^{13} \bar{a}_{\mathrm{p},k} b_k^{13}(\hat{t}) \tag{15}$$

$$a_\mathrm{t}^2(\hat{t}) = \frac{1}{t_\mathrm{f}^4} \left\| \boldsymbol{x}_d'(\zeta(\hat{t}))\theta'(\hat{t}) + \boldsymbol{x}_d''(\zeta(\hat{t}))\theta^2(\hat{t}) \right\|^2 = \sum_{k=0}^{26} \bar{a}_{\mathrm{t},k} b_k^{26}(\hat{t}) \tag{16}$$

$$\sin\gamma(\zeta) = \frac{e_z^\mathsf{T} \boldsymbol{x}_d'(\zeta)}{\sigma(\zeta)} = \frac{\sum_{k=0}^{4} w_{\gamma,k} \bar{\gamma}_k b_k^4(\zeta)}{\sum_{k=0}^{4} w_{\gamma,k} b_k^4(\zeta)} \tag{17}$$

$$\dot{\gamma}^2(\hat{t}) = \left[\frac{\sigma(\zeta(\hat{t}))e_z^\mathsf{T}\boldsymbol{x}_d''(\zeta(\hat{t})) - \sigma'(\zeta(\hat{t}))e_z^\mathsf{T}\boldsymbol{x}_d'(\zeta(\hat{t}))}{\sigma(\zeta(\hat{t})) \left(\left(e_x^\mathsf{T}\boldsymbol{x}_d'(\zeta(\hat{t})) \right)^2 + \left(e_y^\mathsf{T}\boldsymbol{x}_d(\zeta(\hat{t})) \right)^2 \right)^{1/2}} \left(\frac{\theta(\hat{t})}{t_\mathrm{f}} \right) \right]^2 = \frac{\sum_{k=0}^{48} w_{\dot{\gamma},k} \bar{\dot{\gamma}}_k b_k^{48}(\zeta)}{\sum_{k=0}^{48} w_{\dot{\gamma},k} b_k^{48}(\zeta)} \tag{18}$$

*$x_d(t)$ has a Pythagorean hodograph if $x_d'(t) = A(t)\boldsymbol{i}A^*(t)$, where $A(t)$ is a quaternion polynomial of the form $A(t) = u(t) + v(t)\boldsymbol{i} + p(t)\boldsymbol{j} + q(t)\boldsymbol{k}$ [11].

$$\dot{\chi}(\hat{t}) = \frac{e_z^{\mathsf{T}}\left(\boldsymbol{x}_d'(\zeta(\hat{t})) \times \boldsymbol{x}_d''(\zeta(\hat{t}))\right)}{\left(e_x^{\mathsf{T}}\boldsymbol{x}_d'(\zeta(\hat{t}))\right)^2 + \left(e_y^{\mathsf{T}}\boldsymbol{x}_d'(\zeta(\hat{t}))\right)^2}\left(\frac{\theta(\hat{t})}{t_{\mathrm{f}}}\right) = \frac{\sum_{k=0}^{24} w_{\chi,k}\bar{\chi}_k b_k^{24}(\zeta)}{\sum_{k=0}^{24} w_{\chi,k} b_k^{24}(\zeta)}., \tag{19}$$

where $e_x = \begin{bmatrix}1 & 0 & 0\end{bmatrix}^{\mathsf{T}}$, $e_y = \begin{bmatrix}0 & 1 & 0\end{bmatrix}^{\mathsf{T}}$, and $e_z = \begin{bmatrix}0 & 0 & 1\end{bmatrix}^{\mathsf{T}}$.

Additional constraints on path boundary conditions and mission-specified constraints can also be imposed on the trajectories. For multi-vehicle missions, temporal or spatial inter-vehicle separation constraints can also be specified. With the trajectory and constraints defined as above, the optimization framework developed in [7, 9] can be used to generate a feasible trajectory for the vehicle.

IV. Acoustic Noise Model and Constraint

For the purposes of this trajectory generation method, it is assumed that the acoustic power of a single propeller is proportional to the angular speed of the propeller to the tenth power, $p_{rms}^2 \propto \omega_p^{10} \propto M_T^{10}$, where M_t is the Mach number of the propeller tip. The exponent on tip Mach number was obtained from fitting data[†] obtained from the Propeller Analysis System of the Aircraft Noise Prediction Program (PAS-ANOPP) [13]. Disregarding frequency dependence, the overall sound pressure level from a single propeller can be written as $OASPL' \propto 10\log_{10}(M_t^{10}/M_{t,ref}^{10})$, where $M_{t,ref}$ is a reference tip Mach number. It is further assumed that each propeller is an omnidirectional source, with equal acoustic power radiated in all directions. Then, $OASPL' \propto 10\log_{10}((r/r_{ref})^2)$, where r is the distance from the source to an observer and r_{ref} is a reference distance. Under the further simplifying assumtions that the N_p propellers all operated at identical speeds, are incoherent sources (no interference between propellers), and acoustically compact (wavelength is much larger than the distance between propellers), $OASPL \propto 10\log_{10}(Np)$. Combining all the above terms,

$$OASPL = OASPL_{ref}' + 10\log_{10}\left(\frac{M_t^{10}}{M_{t,ref}^{10}}\right) + 10\log_{10}\left(\frac{r_{ref}^2}{r^2}\right) + 10\log_{10}\left(N_p\right), \tag{20}$$

where it is noted that $OASPL_{ref}'$ is the reference value for a single propeller. The acoustic constraint on the OASPL at observer $\mathcal{A}$ is then defined as $OASPL_{\mathcal{A}} \leq OASPL_{max}$. To write an equivalent constraint in terms of parameters derived from the spatial path and speed profile, first rearrange (20) as

$$\frac{M_t^{10}}{r^2} = \frac{M_{t,ref}^{10}}{r_{ref}^2 N_p} 10^{0.1(OASPL_{\mathcal{A}} - OASPL_{ref})}. \tag{21}$$

Substituting $M_t = \omega_p d_p/2c$,(3), and noting that the distance from source to observer can be easily obtained from $r^2 = \|x_d - \mathcal{A}\|^2$, one can find the following relationship between thrust and OASPL:

$$\frac{T^5}{K_T^5 r^2} = \beta_{\mathcal{A}} \triangleq \frac{1024 c^{10} M_{t,ref}^{10}}{d_p^{10} r_{ref}^2 N_p} 10^{0.1(OASPL_{\mathcal{A}} - OASPL_{ref})}. \tag{22}$$

Note that the thrust can be obtained in terms of the trajectory as $T(\hat{t}) = a_p(\hat{t}) + K_D V(\hat{t})$. Since the right hand side is monotonic in the argument $OASPL_{\mathcal{A}} - OASPL_{ref}'$ and that the quantities in the fraction sare constant we can form the equivalent OASPL constraint

$$\beta_{\mathcal{A}}\left(\hat{t}\right) = \frac{T^5\left(\hat{t}\right)}{K_T\left(V\left(\hat{t}\right)\right)^5 r^2\left(\zeta\left(\hat{t}\right)\right)} \leq \beta_{\mathcal{A},max}. \tag{23}$$

Since the denominator is always strictly greater than zero, $\beta_{\mathcal{A}}^2$ can be written as a rational Bézier curve:

$$\beta_{\mathcal{A}}\left(\hat{t}\right) = \frac{\sum_{k=0}^{140} w_{\beta,k}\bar{\beta}_{\mathcal{A},k} b_k^{140}\left(\hat{t}\right)}{\sum_{k=0}^{140} w_{\beta,k} b_k^{140}\left(\hat{t}\right)}, \tag{24}$$

[†]The actual numeric fit value was $M_t^{10.7}$, but M_t^{10} still provides a good fit to the data while being much more convenient for the path-planning framework.

where it has been assumed that $K_T(\cdot)$ can be approximated as linear. For $K_T(\cdot)$ of degree $n_{K_T} \geq 2$, the degree of $\beta_{\mathcal{A}}\left(\hat{t}\right)$ grows as $70n_{K_T} + 10$.

The acoustic model in (20) is a simple model of the noise level at an observer location and can be useful as a rough approximation. A more accurate representation is given by replacing the propeller tip Mach number with the effective Mach number, M_e, which takes the vehicle's airspeed into account [14]:

$$M_e = \frac{M_t}{1 + J(1 - M_t)}, \tag{25}$$

where $J = \frac{2\pi V}{\omega_p d_p}$ is the propeller advance ratio. The OASPL at an observer is then

$$OASPL_{\mathcal{A}} = OASPL'_{ref} + 10\log_{10}\left(\left(\frac{M_e}{M_{e,ref}}\right)^{8.5}\right) + 10\log_{10}\left(\left(\frac{r_{ref}}{r}\right)^2\right) + 10\log_{10}\left(N_p\right). \tag{26}$$

Unfortunately, this expression cannot be represented as a (rational) Bézier curve in the trajectory parameters using the dynamics defined in Section III. In this case, the OASPL constraint could be checked pointwise along the trajectory, however, as a result, there would be no guarantee the constraint is not violated between the pointwise checks.

A. Frequency-Weighted Acoustic Metric

A-weighting [15] is a common frequency-weighted noise metric, used to adjust for the relative loudness of difference frequency perceived by the human ear. The A-weighting scale as a function of frequency is

$$R_A(f) = \frac{12194^2 f^4}{(f^2 + 20.6^2)\left((f^2 + 107.7^2)(f^2 + 737.9^2)\right)^{\frac{1}{2}}(f^2 + 12194^2)} \tag{27}$$

$$A(f) = 20\log_{10}\left(R_A(f)\right) + 2 \tag{28}$$

where the frequency, $f = \omega_p N_B/(2\pi) = M_t c N_B/(\pi d_p)$ and N_B is the number of blades per propeller. Ideally the A-weighted sound pressure level (SPL) calculation would be done with the effective tip Mach number, but as mentioned in the previous section, the result would not be representable as a rational Bézier curve. The expression is therefore approximated with M_t:

$$OASPL_{\mathcal{A}} = 10\log_{10}\left(\frac{1}{\hat{p}^2}\sum_{k=1}^{N_f}\left(\hat{p}^2_{rms,k}\left(\frac{M_t}{M_{t,ref}}\right)^{\xi_k}\right)\left(\frac{\hat{r}}{r}\right)^2\right), \tag{29}$$

where $\hat{\cdot}$ denotes reference values, N_f is the number of frequencies, and ξ_k are obtained from numeric fits of predicted SPL values. While (29) can be manipulated to obtain an equivalent OASPL constraint in rational Bézier curve form, the resulting polynomial expression is of such a high degree as to be prohibitively computationally expensive to work with. The expression could be checked pointwise along the trajectory but, as before, would not be guaranteed to satisfy constraints between points.

The trajectory generation method proposed in this work appears to be limited to relatively simple acoustic models and metrics, though the method is likely to still be useful as low-fidelity means of generating deconflicted trajectories that satisfy acoustic constraints. Alternative trajectory generation approaches may be required when working with other acoustic models/metrics that are either not differentially flat, result in very high-order polynomials, or otherwise cannot be adequately represented in a polynomial structure. Such alternative approaches are the subject of further research.

V. Simulation Example

In this section, we present a simulation example to illustrate the effect of the acoustic constraint on the solution of the trajectory generation problem. Three vehicles are given initial and final positions such that if the vehicles traveled straight-line paths between them, would result in violation of the acoustic constraints and collision due to loss of inter-vehicle separation. Temporal separation is enforced for this example, thus the spatial paths may intersect, but the vehicles cross the intersection points at different times [7]. Boundary conditions and enforced constraint values are specified in Tables 1 and 2, respectively. The trajectories are optimized such that path arc length and speed variation

Table 1 Boundary conditions for the trajectory generation problem.

	Units	Boundary Condition Specification	
		Initial	Final
Position, $\begin{bmatrix} x \\ y \\ altitude \end{bmatrix}$	m	$\left\{ \begin{bmatrix} 0 \\ 0 \\ 5 \end{bmatrix}, \begin{bmatrix} 0 \\ 30 \\ 5 \end{bmatrix}, \begin{bmatrix} 0 \\ -30 \\ 5 \end{bmatrix} \right\}$	$\left\{ \begin{bmatrix} 1000 \\ 1 \\ 10 \end{bmatrix}, \begin{bmatrix} 1000 \\ -15 \\ 10 \end{bmatrix}, \begin{bmatrix} 1000 \\ 15 \\ 10 \end{bmatrix} \right\}$
Speed, V	m/s	27.5	27.5

Table 2 Enforced constraint values for the trajectory generation problem.

	Units	Constraint Value	
		Min	Max
Position, $\begin{bmatrix} x \\ y \\ altitude \end{bmatrix}$	m	$\begin{bmatrix} - \\ - \\ 0 \end{bmatrix}$	$\begin{bmatrix} - \\ - \\ 400 \end{bmatrix}$
Speed, V	m/s	25	35
Heading, ψ	deg	–	–
Heading Rate, $\dot{\psi}$	deg/s	−30	30
Flight Path Angle, γ	deg	−30	30
Flight Path Angle Rate, $\dot{\gamma}$	deg/s	−30	30
Total Acceleration, $\|a_t\|$	m/s^2	–	10
OASPL	dB	–	65
Separation Distance, $\min_{\hat{t}} \left\|x_{d,i}(\hat{t}) - x_{d,j}(\hat{t})\right\|$	m	5	–

are penalized. Figure 1 shows the computed spatial paths and the acoustic footprint on the ground. At each (x, y) point on the ground, the OASPL value shown is the maximum at that point over the entire mission duration. It is assumed that there is no acoustic interaction between vehicles. On the left of Figure 1, no acoustic constraint is enforced, and the peak OASPL at the observer locations is approximately 83 dB. When the acoustic constraint is set to 65 dB, the spatial paths are altered to meet the new constraint, as demonstrated on the right of Figure 1. The vehicles are forced to deviate substantially from a straight line path in order to satisfy the acoustic constraint.

Figure 2 shows the OASPL values at the observer locations as a function of time, both with and without the acoustic constraint. For the case without the acoustic constraint, the maximum OASPL measured at the first observer is approximately 78 dB and the OASPL at the second observer peaks at about 83 dB. When the acoustic constraint is enforced, the peak OASPL at both observers is reduced to the constraint limit, 65 dB. Because the vehicles travel a greater distance at a slower average speed — as shown in Figure 3 — when the acoustic constraint is enforced, the total mission time is greater than when the acoustic constraint is ignored. Hence, the set of traces without the acoustic constraint end at an earlier time. The vehicles all reduce their speed to the minimum allowed in order to satisfy the acoustic constraint. That the minimum speed occurs at $t = 19s$, while the OASPL peaks occur at $t = 12s$ and $t = 27s$, is an artifact of the polynomial structure imposed on the path. The acceleration of vehicles is relatively small and well within the constraint limits, also shown in Figure 3.

The flight path angle, rate of change of flight path angle, and heading rate of change are plotted in Figure 4. There is a significant change in initial and final flight path angles to accommodate the vertical deviation of the trajectories in the presence of the acoustic constraint, but all values are well within constraints. The predicted vehicle motor speed as a function of time is given in Figure 5. With the acoustic constraint enforced, the RPM reduces noticeably to lower the noise at the observer locations. The shape of the RPM trace, where the minimum RPM occurs between the OASPL peaks is again an artifact of the polynomial structure imposed on the problem.

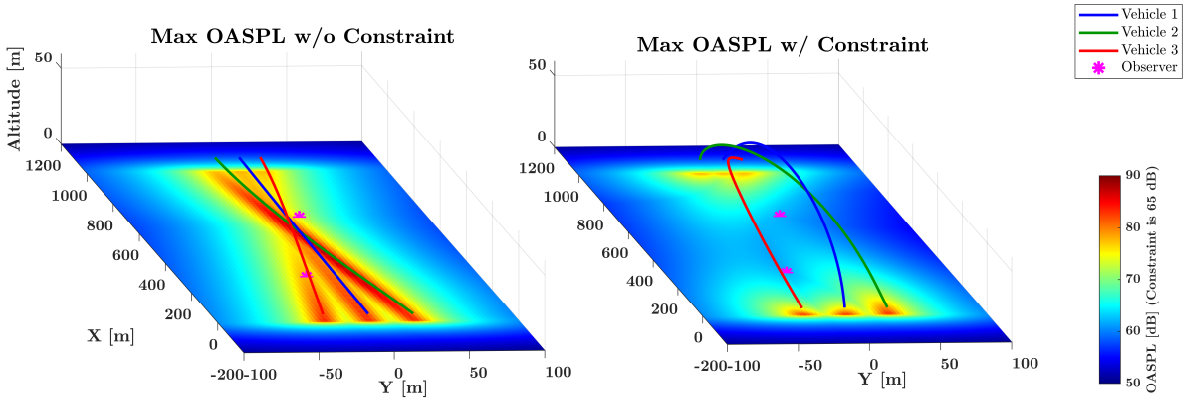

Fig. 1 Maximum OASPL on ground plane without (left) and with (right) acoustic constraint enforced.

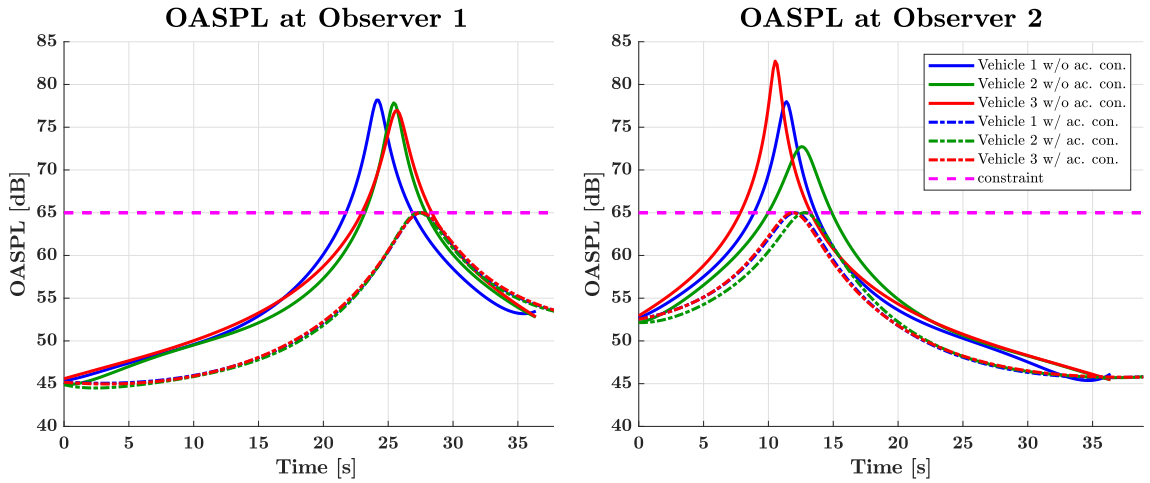

Fig. 2 OASPL value at each observer as a function of mission time.

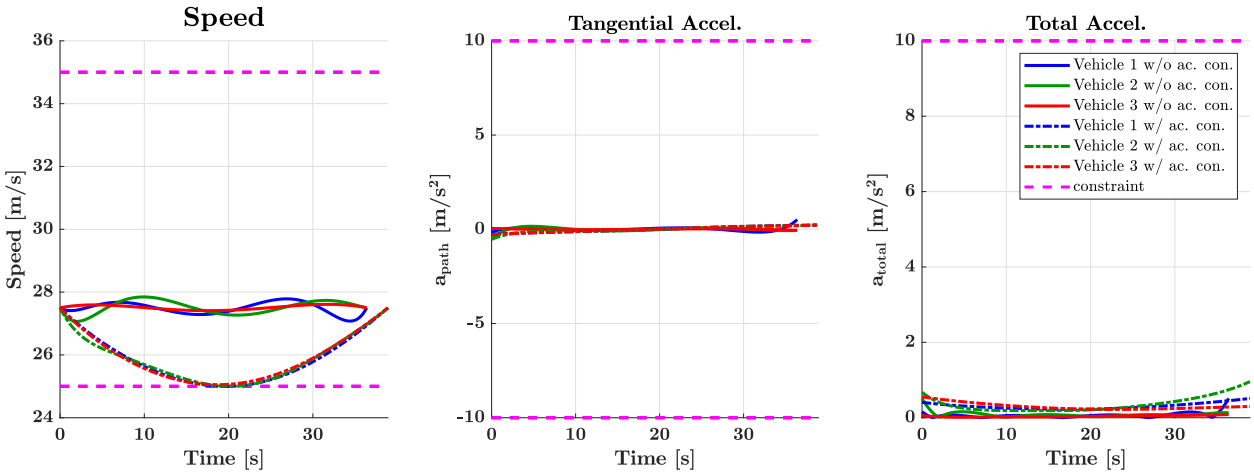

Fig. 3 Vehicle speed and acceleration as a function of mission time.

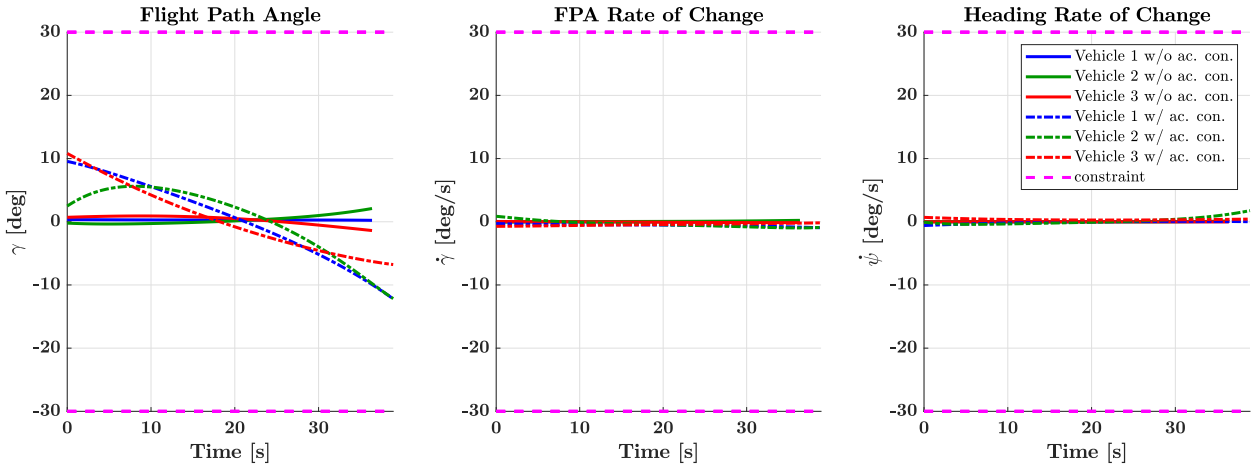

Fig. 4 Flight path angle and rate of change and heading rate of change as a function of mission time.

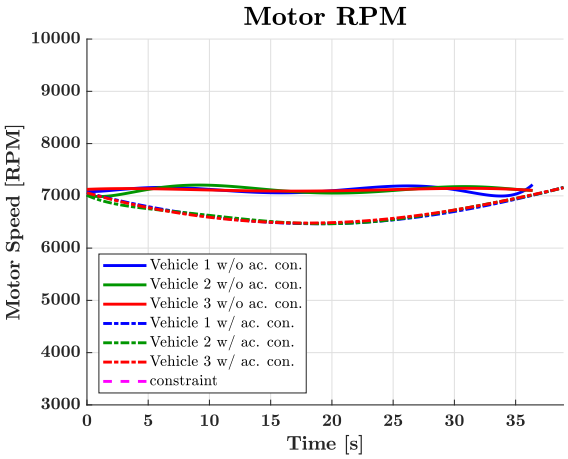

Fig. 5 Predicted vehicle motor speed as a function of mission time.

VI. Conclusion

This paper presented a method for generating trajectories that satisfy acoustic constraints at multiple observer locations. The acoustic model and metric were implemented within an existing framework for cooperative trajectory generation that provides collision-free trajectories for multiple vehicles. The acoustic model and constraint function were formulated as (rational) Bézier curves for computation efficiency and to avoid discretization. A simulation example demonstrated the modification to the trajectories required to satisfy the noise constraints. While the proposed trajectory generation method works well for simple acoustic models and metrics, more sophisticated models and metrics may violate the assumption of differential flatness, result in very high degree polynomials that are computationally expensive to work with, or otherwise not fit well into the polynomial structure imposed by the trajectory generation method. Alternative methods for trajectory generation may be required to work with more sophisticated acoustics model and metrics and are the subject of further research.

Appendix

A. Bézier Curves Background

The Bernstein polynomial basis is defined as

$$b_k^n(\zeta) = \binom{n}{k}(1-\zeta)^{n-k}\zeta^k, \quad \zeta \in [0,1]. \tag{30}$$

A Bézier curve $\boldsymbol{c}(\zeta)$ of degree n and dimension d is defined as

$$\boldsymbol{c}(\zeta) = \sum_{k=0}^{n} \bar{\boldsymbol{c}}_k b_k^n(\zeta), \quad \zeta \in [0,1], \quad \bar{\boldsymbol{c}}_k \in \mathbb{R}^d. \tag{31}$$

A rational Bézier curve $\boldsymbol{r}(\zeta)$ of degree n and dimension d is defined as

$$\boldsymbol{r}(\zeta) = \frac{\sum_{k=0}^{n} w_k \bar{\boldsymbol{r}}_k b_k^n(\zeta)}{\sum_{k=0}^{n} w_k b_k^n(\zeta)}, \quad \zeta \in [0,1], \quad \bar{\boldsymbol{r}}_k \in \mathbb{R}^d, \quad w_k > 0,\ w_k \in \mathbb{R}. \tag{32}$$

Let $\boldsymbol{f}(\zeta)$, $\boldsymbol{g}(\zeta)$ be Bézier curves of degree n and dimension d and let $s(\zeta)$ be a scalar Bézier curve of degree m and $w(\zeta)$ a scalar degree n Bézier curve with $\bar{w}_k > 0$. Select mathematical operations on Bézier curves are then accomplished via the following methods [9].

- **Addition:** $\boldsymbol{h}(\zeta) = \boldsymbol{f}(\zeta) + \boldsymbol{g}(\zeta) = \sum_{k=0}^{n} \bar{\boldsymbol{h}}_k b_k^n(\zeta)$, where $\bar{\boldsymbol{h}}_k = \bar{\boldsymbol{f}}_k + \bar{\boldsymbol{g}}_k$.
- **Subtraction:** $\boldsymbol{h}(\zeta) = \boldsymbol{f}(\zeta) - \boldsymbol{g}(\zeta) = \sum_{k=0}^{n} \bar{\boldsymbol{h}}_k b_k^n(\zeta)$, where $\bar{\boldsymbol{h}}_k = \bar{\boldsymbol{f}}_k - \bar{\boldsymbol{g}}_k$.
- **Multiplication:** $\boldsymbol{h}(\zeta) = \boldsymbol{f}(\zeta)s(\zeta) = \sum_{k=0}^{n+m} \bar{\boldsymbol{h}}_k b_k^{n+m}(\zeta)$, where $\bar{\boldsymbol{h}}_k = \sum_{k=\max(0,k-n)}^{\min(m,k)} \frac{\binom{m}{j}\binom{n}{k-j}}{\binom{m+n}{k}} \bar{\boldsymbol{f}}_{k-j}\bar{s}_j$.
- **Division:** $\boldsymbol{h}(\zeta) = \boldsymbol{f}(\zeta)/w(\zeta) = \frac{\sum_{k=0}^{n} \bar{w}_k \bar{\boldsymbol{h}}_k b_k^n(\zeta)}{\sum_{k=0}^{n} \bar{w}_k b_k^n(\zeta)}$, where $\bar{\boldsymbol{h}}_k = \bar{\boldsymbol{f}}_k/\bar{w}_k$. Note that $\boldsymbol{h}(\zeta)$ is a rational Bézier curve.
- **Differentiation:** $\boldsymbol{h}(\zeta) = \boldsymbol{f}'(\zeta) = \frac{\mathrm{d}}{\mathrm{d}\zeta}\boldsymbol{f}(\zeta) = \sum_{k=0}^{n-1} \bar{\boldsymbol{h}}_k b_k^{n-1}(\zeta)$, where $\bar{\boldsymbol{h}}_k = n(\bar{\boldsymbol{f}}_{k+1} - \bar{\boldsymbol{f}}_k)$.
- **Integration:** $\boldsymbol{h}(\zeta) = \int \boldsymbol{f}(\zeta) = c_0 + \sum_{k=0}^{n+1} \bar{\boldsymbol{h}}_k b_k^{n+1}$, where $\bar{\boldsymbol{h}}_k = \frac{1}{n+1}\sum_{j=0}^{k+1} \bar{\boldsymbol{f}}_k$ for $k = 1, \ldots, n+1$. The control point $\bar{\boldsymbol{h}}_0$ and integration constant c_0 are calculated from the boundary conditions $\boldsymbol{h}(0)$ and $\boldsymbol{h}(1)$.
- **Composition:** $\boldsymbol{h}(\zeta) = \boldsymbol{f}(s(\zeta)) = \sum_{k=0}^{nm} \bar{\boldsymbol{h}}_k b_k^n(\zeta)$, where $\bar{\boldsymbol{h}}_k = \bar{\boldsymbol{H}}_{0,k}^n$, $\bar{\boldsymbol{H}}_{i,0}^0 = \bar{\boldsymbol{f}}_i$, and
$$\bar{\boldsymbol{H}}_{i,k}^j = \frac{1}{\binom{jm}{k}} \sum_{l=\max(0,k-m)}^{\min(k,m(j-1))} \binom{m(j-1)}{l}\binom{m}{k-l}\left[(1-\bar{s}_{k-l})\bar{\boldsymbol{H}}_{i,l}^{j-1} + \bar{s}_{k-l}\bar{\boldsymbol{H}}_{i+1,l}^{j-1}\right].$$
- **Degree elevation:** $\boldsymbol{h}(\zeta) = \sum_{k=0}^{n+m} \bar{\boldsymbol{h}}_k b_k^{n+m}(\zeta) = \boldsymbol{f}(\zeta) = \sum_{k=0}^{n} \bar{\boldsymbol{f}}_k b_k^n(\zeta)$, where $\bar{\boldsymbol{h}}_k = \sum_{j=\max(0,k-m)}^{\min(n,k)} \frac{\binom{m}{k-j}\binom{n}{j}}{\binom{n+m}{k}} \bar{\boldsymbol{f}}_j$.

Additional properties of Bézier curves may be found in [11].

Acknowledgments

The authors would like to thank Kyle Pascioni of NASA Langley Research Center for developing the simplified acoustic models in Section IV and Javier Puig Navarro of NASA Langley Research Center for supplying software for computation of minimum separation between Bézier curves.

References

[1] Vascik, P. D., and Hansman, R. J., "Scaling Constraints for Urban Air Mobility Operations: Air Traffic Control, Ground Infrastructure, and Noise," *2018 Aviation Technology, Integration, and Operations Conference*, 2018.

[2] Whiteside, S. K. S., Zawodny, N. S., Fei, X., Pettingill, N. A., Patterson, M. D., and Rothhaar, P. M., "An Exploration of the Performance and Acoustic Characteristics of UAV-Scale Stacked Rotor Configurations," *AIAA Scitech Forum*, 2019.

[3] Greenwood, E., "Helicopter Flight Procedures for Community Noise Reduction," *73rd American Helicopter Society Annual Forum*, 2017.

[4] Galles, M. B., and Newman, B., "Reducing Noise Impact of Small Aircraft through Indirect Trajectory Optimization," *AIAA Unique and Transformational Flight Conference*, 2020.

[5] Pascioni, K. A., Rizzi, S. A., and Schiller, N., "Noise Reduction Potential of Phase Control for Distributed Propulsion Vehicles," *AIAA Scitech Forum*, 2019.

[6] Patterson, A., Ackerman, K., Gahlawat, A., Hovakimyan, N., Schiller, N. H., and Gregory, I. M., "Controller Design for Propeller Phase Synchronization with Aeroacoustic Performance Metrics," *AIAA Scitech Forum*, 2020.

[7] Choe, R., Puig-Navarro, J., Cichella, V., Xargay, E., and Hovakimyan, N., "Cooperative Trajectory Generation using Pythagorean Hodograph Bézier curves," *Journal of Guidance, Control, and Dynamics*, 2016, pp. 1744–1763.

[8] Kaminer, I., Pascoal, A., Xargay, E., Hovakimyan, N., Cichella, V., and Dobrokhodov, V., *Time-Critical Cooperative Control of Autonomous Air Vehicles*, Elsevier, 2017.

[9] Choe, R., "Distributed Cooperative Trajectory Generation for Multiple Autonomous Vehicles using Pythagorean Hodograph Bézier Curves," Ph.D. thesis, University of Illinois at Urbana-Champaign, 2017.

[10] Rothhaar, P. M., Murphy, P. C., Bacon, B. J., Gregory, I. M., Grauer, J. A., Busan, R. C., and Croom, M. A., "NASA Langley Distributed Propulsion VTOL TiltWing Aircraft Testing, Modeling, Simulation, Control, and Flight Test Development," *14th AIAA Aviation Technology, Integration, and Operations Conference*, 2014.

[11] Farouki, R. T., *Pythagorean-Hodograph Curves*, Springer, 2008.

[12] Chang, J.-W., Choi, Y.-K., Kim, M.-S., and Wang, W., "Computation of the Minimum Distance Between Two Bézier Curves/Surfaces," *Computers & Graphics*, Vol. 35, No. 3, 2011, pp. 677–684.

[13] Nguygen, L. C., and Kelly, J. J., "A Users Guide for the NASA ANOPP Propeller Analysis System," Tech. Rep. NASA-CR-4768, NASA, 1997.

[14] Pascioni, K., and Rizzi, S. A., "Tonal Noise Prediction of a Distributed Propulsion Unmanned Aerial Vehicle," *AIAA/CEAS Aeroacoustics Conference*, 2018.

[15] McCurdy, R. G., "Tentative standards for sound level meters," *Electrical Engineering*, Vol. 55, No. 3, 1936, pp. 260–263. doi:10.1109/EE.1936.6540526.